Analysis of Coupled Tilted Slot Antennas in FDTD Using a Novel Time Domain Huygens Method With Application to Body Area Networks

Sema Dumanli, *Member, IEEE*, and Chris J. Railton, *Member, IEEE*

***Abstract*—Despite the undoubted versatility and effectiveness of the finite-difference time-domain (FDTD) method and its enhancements, there remain some problems which require more computer power than is practical. An example of such a problem is the coupling between two or more tilted antennas in the presence of a scattering environment such as is encountered in a body area network (BAN). The dual challenge of a wide range of scales and complicated structures which are not aligned with a Cartesian mesh are addressed using a novel Time Domain Huygens (TDH) approach. Results and comparisons with measurements are presented showing the effectiveness of the method. In addition, the measured and predicted variations of BAN propagation characteristics with body size are investigated.**

***Index Terms*—Body area network (BAN) measurements, finite-difference time-domain (FDTD).**

I. Introduction

THE finite-difference time-domain (FDTD) method has enjoyed ever increasing popularity since its inception in 1966 [1] and throughout its subsequent development from that time until today [2]. Despite its great success, there remain problems which require more computer power than is practical and which, therefore, present a need for improved algorithms. One such problem occurs when the structure to be analyzed is electrically large and contains fine geometrical detail. To model such structures in FDTD, a large and dense mesh is needed which, in turn, creates a very high computational load. The challenge is very much increased if parts of the structure are not aligned with the Cartesian FDTD grid. This can happen, for instance, if the propagation channel between two or more antennas is to be modeled in a situation such as the body area network (BAN) shown in Fig. 1. The antennas can be oriented arbitrarily and, therefore, even if each of them is individually well behaved in terms of its conformability with a Cartesian mesh, the overall structure is not.

Some ways of solving large problems containing areas of fine detail have been suggested, such as subgridding [3], [4] in which the total problem is split into a number of connected smaller problems, each of which is readily amenable to available FDTD methods. The subproblems can then connected using Huygens surfaces and with various interpolation schemes. However, the subgridding method is unfortunately prone to late time instability and can be difficult to apply to realistic structures. An alternative approach, which avoids the instability problem, is described in [5], [6] and [7]. It is shown to be effective for situations where multiple coupling between the antennas is not significant.

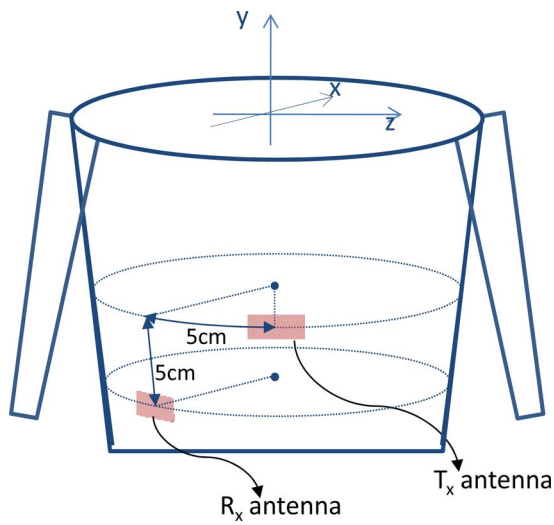

Fig. 1. Transmit and receive antennas located on the body surface representing the body area network considered in the paper.

However, these methods have, so far only been demonstrated for the case where all the subproblems are aligned with the same Cartesian axes. They are, therefore, not suitable to scenarios such as Fig. 1. In this paper, a new method is described which is capable of tackling problems where the antenna elements are arbitrarily orientated with respect to each other and to the underlying Cartesian mesh. The effectiveness of the method is demonstrated by comparison with measurements and also, where possible, with comparison with the, much more computationally expensive, basic FDTD method.

The novel approach is founded on the idea that the Huygens snapshots can be modeled as a mesh of wires which carry the equivalent electric and magnetic currents. By using adapted versions of the methods described in [8], [9], and [10] for slanted wires within the FDTD mesh, the slanted Huygens snapshots

Manuscript received May 10, 2011; revised August 09, 2011; accepted September 23, 2011. Date of publication January 31, 2012; date of current version April 06, 2012.

S. Dumanli is with Toshiba Research Europe, Ltd., Bristol BS1 4ND, U.K. (e-mail: sema.dumanli@toshiba-trel.com).

C. J. Railton is with the Centre for Communications Research, University of Bristol, Bristol BS8 1BU, U.K. (e-mail: chris.railton@bristol.ac.uk).

Color versions of one or more of the figures in this paper are available online at http://ieeexplore.ieee.org.

Digital Object Identifier 10.1109/TAP.2012.2186256

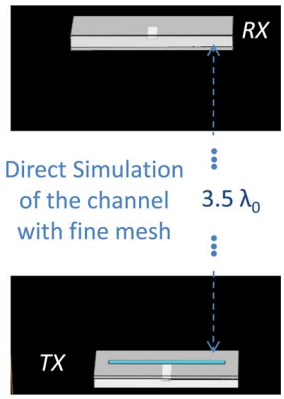

Fig. 2. 5.2-GHz channel model, full channel is modeled with fine mesh in order to cover the details of the antennas, largest unit cell = 1.5 mm, smallest unit cell = 0.2 mm, λ_0 = 57.7 mm.

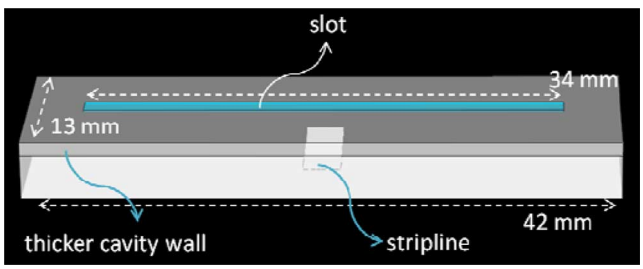

Fig. 3. 5.2 GHz slot, slot length = 34 mm, cavity width = 13 mm, cavity length = 42 mm, cavity thickness = 3.15 mm. Upper wall of the cavity is thicker than they are in reality in order to resolve it using coarse mesh.

can be effectively modeled. A number of practical implementation issues exist for this method and these, and their effects on final accuracy and efficiency, are discussed.

II. Basic Time-Domain Huygens Approach

The basic TDH method has been described in the literature, e.g., [5]–[7], [11] so only a brief summary is given here. As an example, consider the data link shown in Fig. 2. Here there are two terminals, each incorporating a cavity backed slot (CBS) antenna as shown in Fig. 3. These are separated by a distance of $3.5\lambda_0$ (free space wavelength). It is desired to find the coupling between the two antennas in the presence of a scattering environment.

In order to reduce the amount of computer resources needed to analyze the link, the scenario shown in Fig. 2 is split into three sections. These are illustrated in Fig. 4 and are described as follows:

1) The transmit antenna is simulated in isolation using a fine mesh as before. At each time step of the simulation, the tangential electric and magnetic fields on the slot are recorded and written to a file for later use. Because only a single antenna element is being modeled, the size of the computational domain is small; thus, the amount of computation is much reduced.
2) The full structure is then modeled but with a mesh which is much coarser than would be needed in a direct FDTD simulation, and therefore faster to run. For this step, the details of the antenna do not need to be accurately represented since the Huygens' snapshot, produced in 1) will be used for excitation. During this part of the simulation, the tangential electric and magnetic fields on the slot of the receiving antenna are recorded and written to a file.
3) The receive antenna is then modeled in isolation using a fine mesh and is excited at the slot by the Huygens' snapshot obtained in 2). As in 1), the computational domain in this case is much smaller than for the whole structure so that the required computational resources are much less.

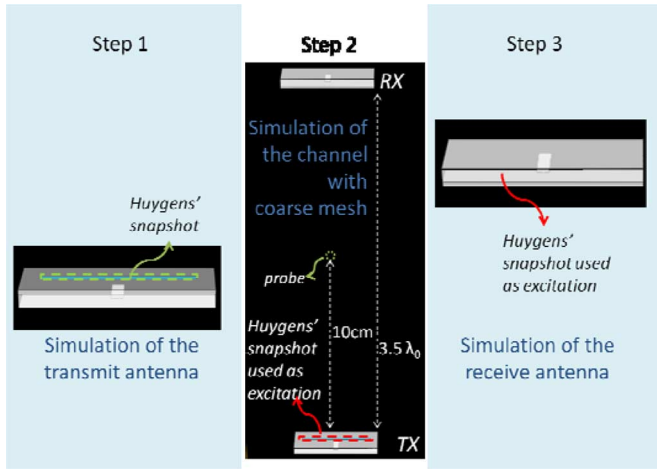

Fig. 4. Three steps of the channel simulation with Huygens' Technique.

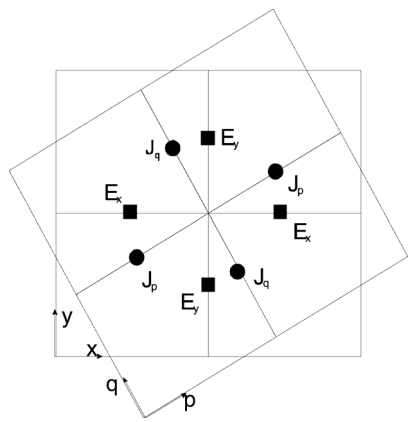

Fig. 5. Huygens snapshot in the (p,q) plane.

III. Application of Time-Domain Huygens When the Surfaces Are Tilted

For situations where all the Huygens' surfaces are aligned with the Cartesian FDTD mesh, the methods described in [5], [6] and [7] can be used. However, where the surfaces are tilted with respect to the mesh, an alternative approach is necessary.

Consider a Huygens snapshot which is to be applied at an angle with respect to the FDTD grid in stage 2 of the algorithm as would be necessary for the situation shown in Fig. 1. As an example, and for clarity, a 2-D scenario for the case of the equivalent electric currents in the snapshot and the E field nodes in the FDTD mesh is shown in Fig. 5. The same principle is directly applicable to a 3-D structure and the H and M nodes are dealt with in a completely analogous way to the E and J nodes. The snapshot equivalent currents are aligned with the (p,q) coordinate system whereas the E field nodes to which they must be

added are lined up with the (x,y) coordinate system. The Huygens snapshot can be considered to be a pair of wire meshes, each segment of which carries an equivalent electric and magnetic current which represent the impressed fields.

Much work has been done to find efficient and accurate ways to represent wires within the FDTD mesh. In 1981, Holland and Simpson presented a thin wire formulation [12] which allowed receiving and transmitting dipole antennas to be efficiently modeled. Later Ledfelt, [13], [14], enhanced the algorithm in order to improve the accuracy for wires orientated at arbitrary angles with respect to the mesh by using a "shell average." This involved estimating the $\boldsymbol{E}$ field around the wire by interpolating from a larger number of $\boldsymbol{E}$ field nodes than used in the tri-linear interpolation [11]. Because the average is taken over a larger area, the shell average is less sensitive to the exact position and orientation of the wires. This approach was further developed by Edelvik, [8] who introduced a raised cosine basis function to represent the current density around the wire. In [15], the effect of the singular nature of the radial electric field and circulating magnetic field was included. It was shown that this technique could be successfully applied to wire transmission lines terminated by resistors and by other structures. In this work, the shell average of [14] is applied separately to each segment of the Huygens snapshot. There are three main differences between the situation here and the original application to wires and wire bundles which need to be considered:

1) In the case of thin wires it is necessary to model the coupling from the wire currents to the FDTD fields and vice versa. However, when using the TDH surface to excite a structure no physical wires exist in which currents would be induced. Therefore, it is only necessary to model the coupling into the FDTD mesh.
2) In the method of [14], the presence of closely spaced wires requires that the mutual inductance between them is included in the calculation. In this case, that is not necessary since there are no physical wires in the model.
3) In order to use a Huygens equivalent surface, there must be both equivalent electric currents (I) and equivalent magnetic currents (M) on that surface. These are approximated by two separate grids of equivalent wires, one grid carrying electric current and the other grid carrying magnetic current. The equivalent wires carrying electric current are modeled using the shell average method as described in [14]. The equivalent wires carrying the magnetic current are modeled in a completely analogous manner with H and M taking the place of E and I.

IV. Application of the Shell Average Method for Time Domain Huygens Excitation

The shell average method of excitation can be illustrated with reference to Fig. 6. Here the FDTD mesh is shown together with an equivalent wire segment which passes through it and carries an equivalent current, I_{w}. To apply the method, a disk is drawn centered at the centre of the wire segment and orientated at right angles to it. Around the circumference of this disk a number of equally spaced points are placed, shown as blue dots on the figure. The current, I_{w}, is treated as if it was shared out equally

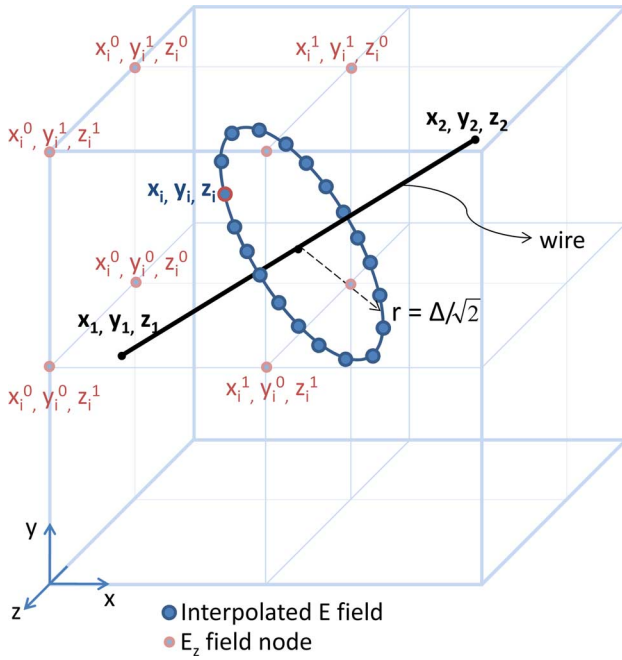

Fig. 6. 3-D illustration of the shell average method of excitation.

between each dot and the current assigned to each dot is applied to the nearest FDTD nodes using tri-linear interpolation.

For instance, consider excitation of the $\mathrm{E_z}$ nodes in the FDTD mesh from an equivalent wire segment which starts at point (x_1, y_1, z_1) and ends at point (x_2, y_2, z_2), then the disk will have a center of $((x_1+x_2)/2, (y_1+y_2)/2, (z_1+z_2)/2)$. Let the coordinates of the ith point on the shell will be $(x_{\mathrm{i}}, y_{\mathrm{i}}, z_{\mathrm{i}})$ then the eight nearest $\mathrm{E_z}$ nodes are given by $(x_{\mathrm{i}}^p, y_{\mathrm{i}}^q, z_{\mathrm{i}}^r)$ where p, q, r can take the values "0" or "1" and

$$x_i^0 = \Delta\left(\mathrm{int}\left(\frac{x_i}{\Delta}\right)\right) \quad x_i^1 = \Delta\left(1+\mathrm{int}\left(\frac{x_i}{\Delta}\right)\right)$$
$$y_i^0 = \Delta\left(\mathrm{int}\left(\frac{y_i}{\Delta}\right)\right) \quad y_i^1 = \Delta\left(1+\mathrm{int}\left(\frac{y_i}{\Delta}\right)\right)$$
$$z_i^0 = \Delta\left(\mathrm{int}\left(\frac{z_i-0.5}{\Delta}\right)\right) \quad z_i^1 = \Delta\left(1+\mathrm{int}\left(\frac{z_i+0.5}{\Delta}\right)\right) \tag{1}$$

and Δ is the FDTD cell size and the function $\mathrm{int}(x)$ returns the largest integer which is less than x.

Consider the point $((x_{\mathrm{i}}, y_{\mathrm{i}}, z_{\mathrm{i}})$ on the shell as shown in Fig. 7. If the equivalent current in the wire is I_{w}, then the part of the current allocated to this point on the shell is I_{w}/N where N is the number of points on the shell. Furthermore, since this allocated current is in the direction of the wire, it can be resolved into the three coordinate axes used by the FDTD mesh as follows:

$$I_{xi} = \frac{1}{N} I_w \frac{x_2 - x_1}{\delta}$$
$$I_{yi} = \frac{1}{N} I_w \frac{y_2 - y_1}{\delta}$$
$$I_{zi} = \frac{1}{N} I_w \frac{z_2 - z_1}{\delta} \tag{2}$$

where δ is the length of the wire segment.

Each component of the current at the shell point is shared out amongst the nearest eight nodes by tri-linear interpolation. For

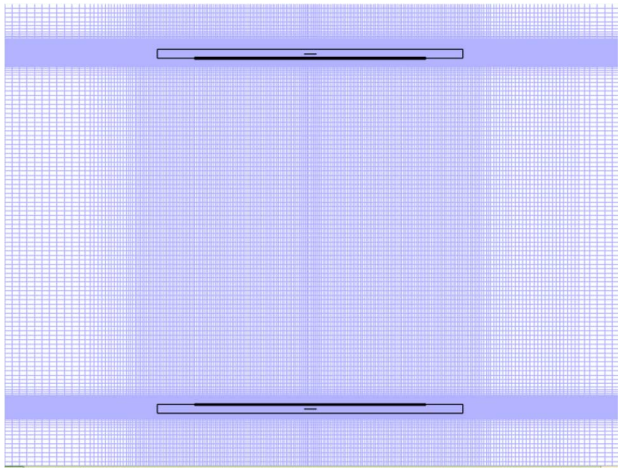

Fig. 7. Mesh used for the direct calculation of coupling: "Direct FDTD."

instance, the z component of the equivalent current applied to the (p,q,r)th FDTD node is given by

$$I_{z(p,q,r)} = I_{zi}\phi\left(x_i, x_i^p\right)\phi\left(y_i, y_i^q\right)\phi\left(z_i, z_i^r\right) \tag{3}$$

where:

$$\phi(u,v) = \begin{bmatrix} \frac{v-u}{\Delta} & v \le u \le v+\Delta \\ \frac{u-v}{\Delta} & v \ge u \ge v-\Delta \\ 0 & \text{elsewhere} \end{bmatrix}. \tag{4}$$

This current can be included in the FDTD update equation for the (p,q,r)th node.

The radius of the shell is a freely chosen parameter. A value of zero corresponds to direct tri-linear interpolation of the current on the wire to the eight nearest FDTD nodes whereas a large value, such as $\Delta/\sqrt{2}$ which has been used for tilted wires [14] spreads the incident energy over a larger number of cells. In contrast to the tilted wire case, it has been found empirically that the best choice of radius in this situation is a small value and direct tri-linear interpolation will give a good result. For the results presented later, a value of $\Delta/10$ has been chosen.

V. Shell Average Method for Generation of Huygens' Snapshots

The generation of snapshots which are tilted with respect to the underlying FDTD mesh can also be done using the shell average method. Again considering Fig. 6, it is now required to estimate the tangential E and H field on the wire segment. In this case the fields at each point on the shell are estimated using tri-linear interpolation from the eight nearest FDTD nodes. The E and H fields on the equivalent wire are then found by averaging the estimated fields on all the dots.

The equivalent currents are then found as

$$I_w = \hat{n} \times H\delta \tag{5}$$

where n is the direction normal to the snapshot plane and δ is the distance between neighboring wires.

The number of points in the Huygens' snapshot is a freely chosen parameter. By default, in the method used in [5], [6] and [7] the snapshot cell size is the same as the cell size of the FDTD mesh. When the snapshots are tilted, and especially if the FDTD mesh is graded, a choice must be made. It has been found that the choice of snapshot size is not critical and choosing the size to be similar to the size of the target FDTD mesh gives good results while keeping the size of the files within reasonable bounds.

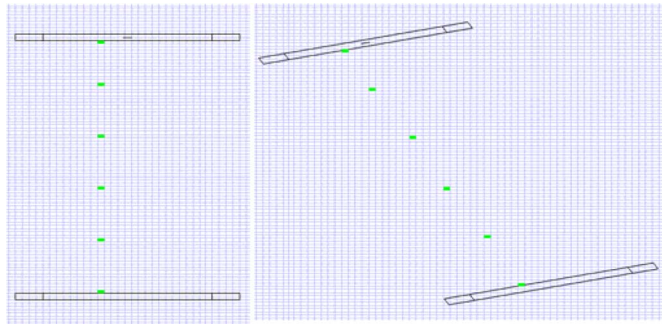

Fig. 8. (a) Mesh used for stage 2 of the TDH method: "TDH No tilt" (b) The mesh used for stage 2 of the TDH method: "TDH Tilted," both elements tilted relative to the FDTD mesh.

VI. Some Other Practical Considerations

Since the antenna elements are slots, it is only necessary to use a Huygens' snapshot which covers the slot itself, rather than having to surround the whole antenna as in [5]. However, this raises two issues. First, although the details of the innards of the antenna do not need to be precisely modeled in Stage 2, the box surrounding the cavity does need to be included. If this box is tilted, and the walls are considered to be very thin, then these cannot be resolved using the coarse FDTD grid. In order to overcome this, it is necessary to make the walls of the cavity thicker than they are in reality. That, combined with the use of the Dey–Mittra algorithm for tilted solid metal objects [16], has been found to give good results.

A second issue raised by the modeling of a CBS element is that the cavity is filled with a dielectric. The Huygens' surface can be taken on a plane infinitesimally above or infinitesimally below the dielectric boundary. However, since the tangential fields are continuous, this makes no difference to the result. When the E field nodes are updated with the values of J on the snapshot, the update is done in accordance with standard FDTD, i.e., using the permittivity of the material in which the target node appears or, if the node is on the boundary, using the average of the permittivities either side of that boundary.

VII. Results for Two Coupled CBS Antennas

In order to show the effect of tilting the antennas on the predicted results, calculated results were produced for the scenario shown in Fig. 3 using the meshes shown in Figs. 7 and 8. Fig. 7 shows the scenario with the antenna elements in parallel with the FDTD mesh and with a mesh suitable for a direct FDTD simulation. Here cell sizes ranged from 1.5 mm to 0.2 mm and the time step was 0.4 ps. Fig. 8(a) shows Stage 2 of the same scenario which requires a much coarser mesh. In this case, the cell size is 1 mm $(\lambda/20)$ was used and the time step was 1.15 ps. Finally, Fig. 8(b) shows the same scenario but with the whole environment tilted by 10° with respect to the FDTD mesh. This model is simulated both with the uniform 1 mm mesh shown in

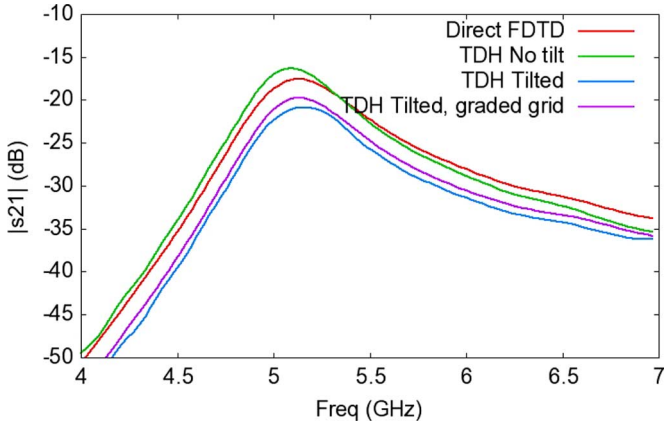

Fig. 9. Transmission coefficient simulated with direct FDTD and FDTD-TDH.

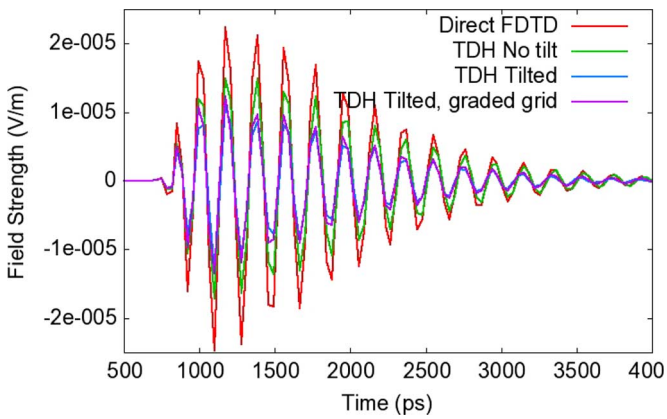

Fig. 10. Received amplitude simulated with direct FDTD and FDTD-TDH.

Fig. 8(b) and also with a graded mesh in which the cells around the antenna elements were reduced to 0.5 mm. The required the time step for the graded mesh is 0.7 ps. In each case the excitation pulse was chosen to be a 5-GHz sine wave modulated by a raised cosine envelope having a width of 200 ps. This gives a good energy density over the frequency range of interest. Note that stage 1 and stage 3 are identical in all the tilted and non-tilted cases. Since the physical arrangement is the same in each case, the results for the coupling between antennas and for the field amplitudes at points between the antennas should be the same. Any differences represent the effects of the lattice properties having been changed.

In Fig. 9, the transmission coefficient simulated with Direct FDTD and FDTD-TDH is shown. Although the Direct FDTD results are very similar to the ones generated with TDH, there is some error associated with the tilting. A second run was done using the graded grid. This will allow the effects of the metal cavity walls and also the precision with which the Huygens' snapshots are recorded and applied to be better modeled. It can be seen that the increase in computational requirement has yielded some increase in accuracy. Time-domain results are shown in Fig. 10. It can be seen that the arrival times of the signal predicted by each method are in good agreement and that there is a small difference in predicted amplitudes.

Details of the computational resources used are shown in Table I. Here it can be seen that, compared to 270 minutes for a direct FDTD run, the TDH runs took a total of 180 minutes for the coarser mesh and 207 minutes for the graded mesh. Thus, there is a moderate saving in computer time even when the elements are aligned with the FDTD grid. However, the main benefit of the method happens when the elements are tilted since, in this case, direct FDTD cannot practically be used as the errors would be severe even with a very fine mesh.

TABLE I
COMPUTATIONAL PARAMETERS FOR DIRECT AND TDH RUNS. ALL RUNS WERE DONE USING AN INTEL CORE 3 PROCESSOR AND SINGLE THREADED CODE

	Cell size (mm)	Time step (ps)	Iterations	Run time (mins)
Direct	0.2 - 1.5	0.45	16000	270
TDH stage 1	0.2 – 1.5	0.45	8000	46
TDH Stage 2	1	1.15	8000	35
TDH stage 2	0.5 - 1	0.7	8000	56
TDH stage 3	0.2 – 1.5	0.45	16000	105

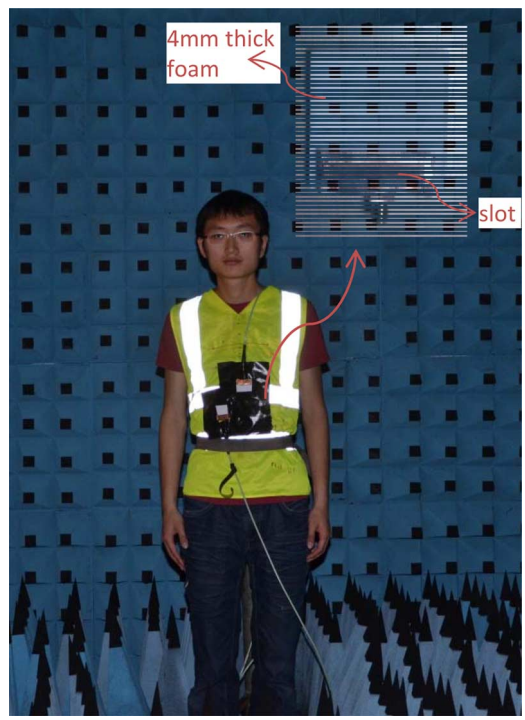

Fig. 11. Measurements setup: slot antennas are fixed on a male subject in the anechoic chamber as shown in Fig. 1.

VIII. AN ON-BODY SCENARIO

The approach is now applied to a real situation of a propagation channel between two antennas placed on a human body. A transmit and a receive antenna is located on the upper body of a male as seen in Fig. 1. The distance between the antennas is 7.07 cm ($= 1.225\lambda$) and the distance between the back of the CBS antennas and the body is 5 mm ($= 0.087\lambda$).

The on-body channel propagation scenario is analyzed at 5.2 GHz with measurements and with the TDH technique. The measurements were taken at 1600 frequency points between 3.5 and 7.5 GHz using a Hewlett Packard 8510 vector network analyzer (VNA) in the anechoic chamber as seen in Fig. 11. For each link, 25 measurements were taken and averaged. Therefore, 225 measurements were taken for each antenna position using nine

TABLE II
PROPERTIES OF THE SUBJECTS UNDER TEST

Subjects	Weight (kg)	Height (cm)	Fat (%)	Age	BMI(kg/m^2)
Subject 1	88.7	180	22.5	27	27.37654
Subject 2	65.7	183	7.5	23	19.61838
Subject 3	74.1	168	20.9	29	26.25425
Subject 4	86.2	174	27	35	28.4714
Subject 5	78.3	168	22.2	28	27.74235
Subject 6	68.4	174	13.5	27	22.59215
Subject 7	90.9	178	24	23	28.68956
Subject 8	80.1	176	19.7	27	25.85873
Subject 9	81.8	180	18.5	26	25.24691

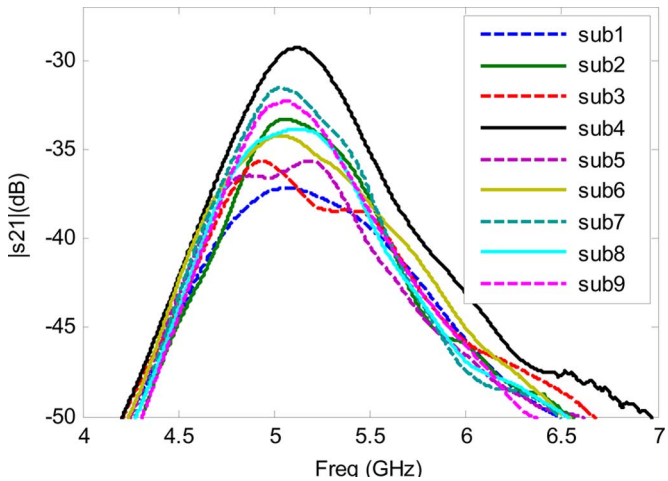

Fig. 12. Measurements on nine different subjects.

different male subjects. General body compositions and heights of the subjects are listed in Table II. Note that all metallic and electrical devices were removed from the subjects and the distance between the antennas and the body is fixed by locating the antennas on a 4-mm-thick foam.

As seen in Fig. 12, the measured channel characteristics change substantially between one person and another. The transmission coefficient at its maximum varies between -29 dB and -37 dB. In order to find out which parameters most influence this variation, a number of FDTD simulations have been done.

A numerical phantom described in [7] is used to simulate the on-body propagation scenario where the upper body of an average male excluding the head was modeled as a cylindrical multi-layered structure using 15 different tissue types. The body parts and organs were approximated by basic geometries such as spheres, cylinders, and cubes.

Since the receive antenna is not aligned with the FDTD mesh, the FDTD-TDH algorithm is essential for this scenario. The scenario cannot practically be simulated with direct FDTD. The same steps described in Section II are followed. Frequency snapshots taken at stage 2 of the simulations for 5.2 GHz are plotted in Figs. 14 and 15. The snapshots are taken on the sagital plane of the body as shown in Fig. 13. They include the lower side wall of the transmit antenna and receive antenna, respectively. In addition to the alignment of the antennas, the

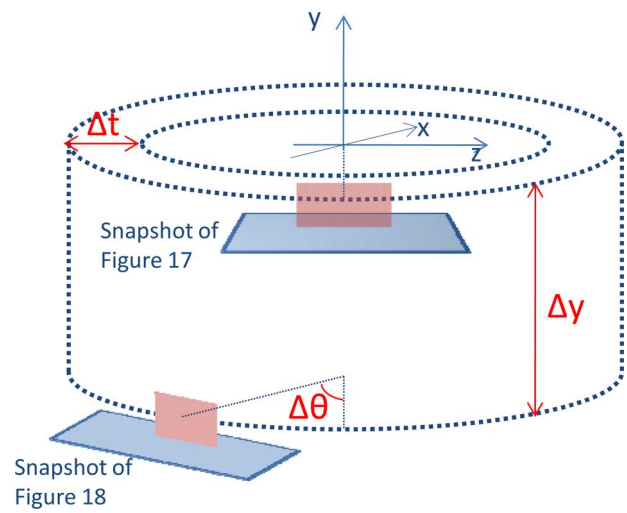

Fig. 13. Positions of the snapshots shown in Figs. 14 and 15 and the applied variations: the thickness of the fat tissue (Δt), the distance between the antennas in the y direction (Δy) and the tilt angle of the receive antenna ($\Delta\theta$).

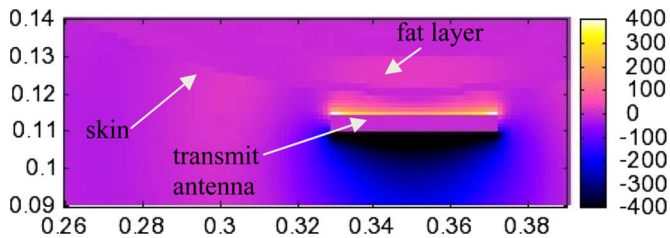

Fig. 14. Real component of the E field on the lower y wall of the transmit antenna on xz plane.

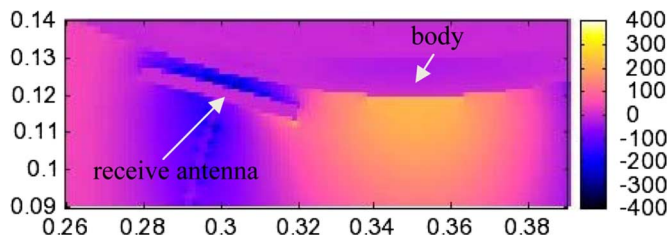

Fig. 15. Real component of the E field on the lower y wall of the receive antenna on xz plane.

evanescence of the E field within the cylindrical phantom can also be observed from these figures.

Simulations were performed in order to see the effect of varying the parameters in a realistic way. The parameters which are varied are the thickness of the fat tissue (Δt), the distance between the antennas in y direction (Δy) and the tilt angle of the receive antenna ($\Delta\theta$) as seen in Fig. 13.

In the first set of simulations Δy is fixed at 5 cm $\Delta\theta$ is fixed at 16° with fat thicknesses of between 3 and 23 mm. Fig. 16 demonstrates how the fat thickness is changed while the other parameters are kept constant.

In the second set of simulations, more realistic variations have been applied as listed in Table III. In this case, as the fat thickness, $\Delta\ t$, is changed from 3 to 18 mm, the length of arc between the antennas kept constant. This is shown in Fig. 17 and is what happens when people with different fat indices wear the adjustable vest on which the antennas are attached. Note that during these variations, the tilt angle of the receive antenna has changed between 14.4° and 19.4°, Δy is fixed at 5 cm, and the

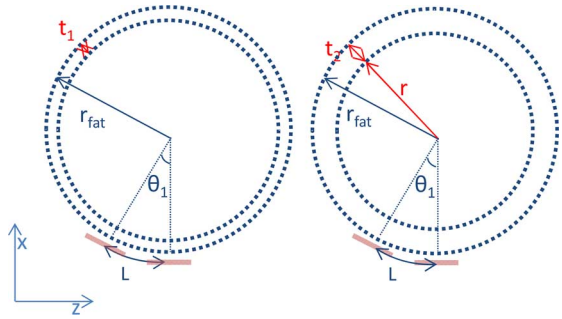

Fig. 16. Thickness of the fat layer is changed by changing the inner radius r so that all the other parameters: θ, L and outer radius r_{fat} are kept constant.

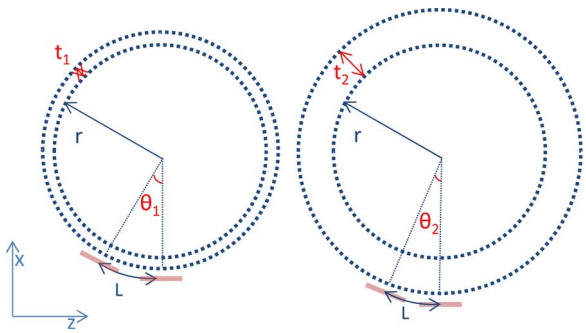

Fig. 17. Realistic fat variations in line with the measurements: t_1 and t_2 represent the changing fat thickness. The parameters r and L are kept constant while t and θ are changed.

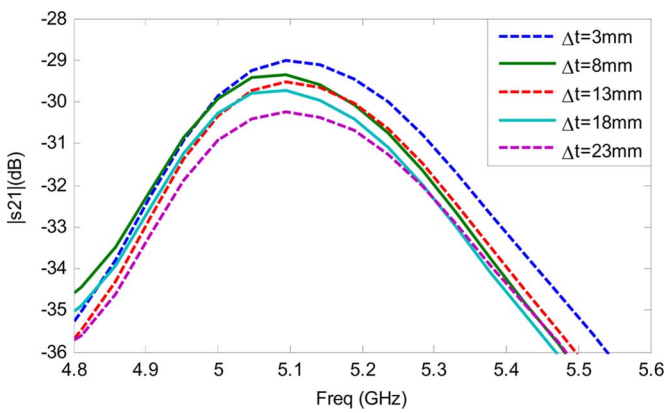

Fig. 18. First set of FDTD-TDH simulations demonstrating the effects of fat variation on the received power. Five different fat thicknesses were considered changing from 3 to 23 mm. Δy is set to 5 cm $\Delta\theta$ is set to 16°.

distance between the antennas and the body is fixed at 5 mm. Δy and $\Delta\theta$ are also changed to represent the errors while attaching the antennas on the vest. During Δy variations, $\Delta\theta$ is set to 16° and Δt is set to 3 mm. Δy is set to 5 cm, Δt is set to 3 mm while varying $\Delta\theta$.

Fig. 18 demonstrates the effects of fat tissue thickness under these conditions on the received power. A small decrease has been observed in the received power as the fat thickness is increased. Maximum received power stayed between -30.5 dB and the original maximum power of -29 dB.

Fig. 19 demonstrates the effect of the variations listed in Table III. The transmission coefficient at its maximum is -28.5 dB when $\Delta y = 4$ cm. This is when the antennas are closest to each other. The weakest signal was received when $\Delta\varphi$ is 19.5°. Corresponding measurements shown in Fig. 12

TABLE III
VARIATIONS DURING BAN SIMULATIONS

Variation	Minimum value	Maximum value	Step
Δt	3mm	18mm	5mm
Δy	4cm	6cm	10mm
$\Delta\theta$	16^0	19.5^0	1.75^0

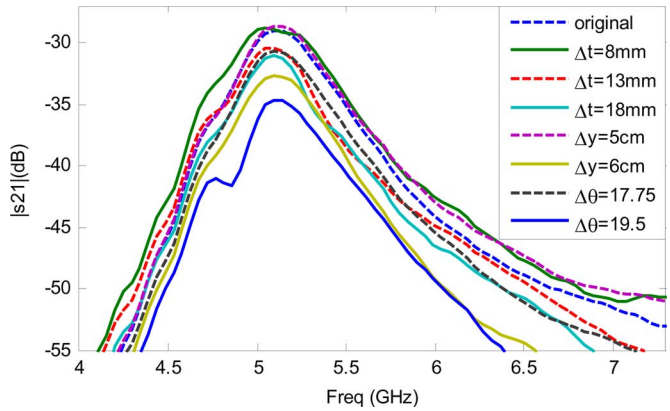

Fig. 19. Second set of FDTD-TDH simulations with variations as listed in Table III and shown in Fig. 17.

are in excellent agreement with Fig. 19, confirming the effectiveness of the FDTD-TDH simulations. In addition to the correct predictions, FDTD-TDH allows the user to change a specific parameter while keeping the others constant which is not possible with measurements.

IX. CONCLUSION

A novel algorithm has been demonstrated for computationally heavy scenarios which contain antennas which are tilted with respect to the FDTD mesh. The algorithm has been verified by basic simulations as well as with measurements and simulations of a realistic BAN scenario. FDTD simulations enhanced with the new algorithm have been performed by using a numerical upper male body phantom and two slot antennas which are tilted according to each others' axes. The simulations have been verified with measurements taken on nine different male subjects. The measured and simulated transmission coefficients have been shown to agree and the practicality and the accuracy of the algorithm have been proved.

ACKNOWLEDGMENT

The authors would like to thank their colleagues W. Thompson and R. Cepeda for their help in taking the measurements.

REFERENCES

[1] K. Yee, "Numerical solution of initial boundary value problems involving maxwell's equations in isotropic media," *IEEE Trans. Antennas and Propagation*, vol. 14, no. 5, pp. 302–307, May 1966.
[2] A. Taflove and S. C. Hagness, *Computational Electrodynamics: The Finite Difference Time Domain Method*, 3rd ed. Norwood, MA: Artech House, 2005, ISBN 1-58053-832-0.
[3] J. P. Berenger, "Three dimensional Huygens subgridding for FDTD," in *Proc. IEEE Int. Symp. Antennas Propag.*, Jun. 2009, pp. 1–4.

[4] J. P. Berenger, "Extension of the Huygens subgridding algorithm to two dimensions," *IEEE Trans. Antennas Propag.*, vol. 57, no. 12, pp. 3860–3867, Dec. 2009.
[5] C. Miry, R. Loison, and R. Gillard, "An efficient bilateral dual-grid-FDTD approach applied to on-body transmission analysis and specific absorption rate computation," *IEEE Trans. Microw. Theory Tech.*, vol. 58, no. 9, pp. 2375–2382, Sep. 2010.
[6] R. Pascaud, R. Gillard, R. Loison, J. Wiart, and M. F. Wong, "Dual grid finite-difference time-domain scheme for the fast simulation of surrounded antennas," *IET Microw. Antennas Propag.*, vol. 1, no. 3, pp. 700–706, Jun. 2007.
[7] S. Dumanli and C. J. Railton, "On-body transmission at 5.2 GHz: Simulations using FDTD with a time domain Huygens' technique," *IEEE Trans. Antennas Propag.*, vol. 59, no. 10, pp. 3910–3917, Oct.. 2011.
[8] F. Edelvik, "A new technique for accurate and stable modeling of arbitrarily oriented thin wires in the FDTD method," *IEEE Trans. Electromag. Compat.*, vol. 45, no. 2, pp. 416–423, May 2003.
[9] G. Zhang and C. J. Railton, "Treatment of arbitrarily-orientated multiwire bundles and terminated multiwire transmission lines in FDTD method," *IET Proc. Microw., Antennas Propag.*, vol. 1, no. 2, pp. 381–387, 2007.
[10] K. Ren and C. J. Railton, "Modelling of microstrip circuit using a hybrid PEEC/FDTD approach," *IEEE Trans. Antennas Propag.*, vol. 56, no. 10, pp. 3253–3259, Oct. 2008.
[11] S. Dumanli, C. J. Railton, and D. L. Paul, "FDTD channel modelling with time domain Huygens' technique," in *Proc. Eur. Conf. Antennas Propag. (EuCAP)*, Rome, Apr. 11–15, 2011, pp. 86–89.
[12] R. Holland and L. Simpson, "Finite-difference analysis of EMP coupling to thin struts and wires," *IEEE Trans. Electromagn. Compat.*, vol. EMC-23, no. 2, pp. 88–97, May 1981.
[13] G. Ledfelt, "Hybrid time-domain methods and wire models for computational electromagnetics," Ph.D. Dissertation, Dept. of Numer. Anal. Comput. Sci., Royal Inst. of Technol., Stockholm, Sweden, 2001.
[14] G. Ledfelt, "A stable subcell model for arbitrarily oriented thin wires for the FDTD method," *Int. J. Numer. Modelling: Electron. Netw., Devices Fields*, vol. 15, pp. 503–515, 2002.
[15] B. P. Koh, C. J. Railton, and I. J. Craddock, "Wire above ground plane transmission line formulation in FDTD algorithm," *Proc IEE-Microw. Antennas Propag.*, vol. 151, no. 3, pp. 249–255, 2004.
[16] S. Dey and R. Mittra, "A locally conformal finite-difference time domain algorithm for modelling three-dimensional perfectly conducting objects," *IEEE Microw. Guid. Wave Lett.*, pp. 273–275, Jul. 1997.

Sema Dumanli (M'11) was born in Elazig, Turkey, in 1984. She received the B.Sc. (first class honors) degree in electrical and electronic engineering from Middle East Technical University (METU), Ankara, Turkey, in 2006 and the Ph.D. degree from University of Bristol, Bristol, U.K., in 2010.

She was with ASELSAN, Inc., Turkey, from 2006 to 2007 as a Design Engineer. She is currently with Toshiba Research Europe, Bristol, U.K., as a Research Engineer. Her research interests include antenna design and propagation channel modeling, for the applications to MIMO, millimeter-wave technology and BAN.

Dr. Dumanli is a member of the IEEE Antennas and Propagation Society. She was the recipient of the Scientific and Technological Research Council of Turkey (TUBITAK) Ph.D. Scholarship and Ph.D. sponsorship of Toshiba Research Europe.

Chris Railton (M'88) received the B.Sc. degree in physics with electronics from the University of London, London, U.K., in 1974 and the Ph.D. degree in electronic engineering from the University of Bath, Bath, U.K., in 1988.

From 1974 to 1984, he worked with the scientific civil service on a number or research and development projects in the areas of communications, signal processing, and EMC. From 1984 to 1987, he was with the University of Bath working on the mathematical modeling of boxed microstrip circuits. He currently works in the Centre for Communications Research, University of Bristol, Bristol, U.K., where he leads the Computational Electromagnetics Team which is engaged in the development of new algorithms for electromagnetic analysis and their application to a wide variety of situations including planar and conformal antennas, microwave and RF heating systems, radar and microwave imaging, EMC, high-speed interconnects, and the design of photonic components.